MOLEKUL
eISSN: 2503-0310

Articles
https://doi.org/10.20884/1.jm.2025.20.2.9097

In Silico Study of Bioactive Compounds from Some Tropical Trees as Inhibitors of Papain-Like Protease SARS-COV-2

Syamsul Falah*, Shobiroh Nuur'Alimah, Laksmi Ambarsari

Department of Biochemistry, Faculty of Mathematics and Natural Sciences, IPB University, Bogor 16680, Indonesia 16680

*Corresponding author email: syamsulfa@apps.ipb.ac.id

Received July 09, 2023; **Accepted** March 10, 2025; **Available online** July 20, 2025

ABSTRACT. Severe Acute Respiratory Syndrome Coronavirus-2 (SARS-CoV-2) is the causal virus of the global COVID-19 pandemic. Furthermore, it is known to encode 4 structural and 16 non-structural proteins, one of which is Papain-Like protease (PLpro). This protein is an essential enzyme that plays a role in the maturation of viral polyproteins, the formation of replicate-transcriptase, and the signaling of the host's innate immune response to viral infections. To prevent the activities of PLpro, several compounds with inhibitory effects have been developed from natural sources. Flavonoid compounds from bay leaf (*Syzygium polyanthum*) and mahogany bark (*Swietenia macrophylla*), as well as phenolics from white teak bark (*Gmelina arborea* Roxb.), have been reported to have antiviral activities, but there are no studies on their potential as PLpro SARS-CoV-2 inhibitors. Therefore, this study aimed to investigate the PLpro SARS-CoV-2 inhibitory effects of 11 bay leaf, 3 mahogany bark, and 6 white teak bark test ligands within silico method using YASARA and PLANTS. The best test ligands obtained were epigallocatechin-3-gallate (-98.93 kcal/mol), catechin (-80.10 kcal/mol), epicatechin (-80.12 kcal/mol), and balanophonin (-83.36 kcal/mol) based on energy binding values surpassing the reference ligands ribavirin (-74.06 kcal/mol) and benserazide (-90.93 kcal/mol). Additionally, these four ligands satisfied physicochemical, pharmacokinetic, and toxicity predictions, in contrast to the natural ligand VIR251, which carries the risk of inhibiting hERG, potentially resulting in fatal outcomes. Based on the results, the compounds could be developed as effective alternative drugs in inhibiting PLpro SARS CoV-2.

Keywords: Covid 19, molecular docking, Papain-Like protease, SARS CoV-2,

INTRODUCTION

Severe Acute Respiratory Syndrome Coronavirus 2 (SARS-CoV-2) is the virus responsible for the Coronavirus Disease 2019 (COVID-19). It was first identified in Wuhan, Hubei Province, China, in December 2019, and quickly spread around the world. This led to its designation as a global pandemic by the World Health Organization (WHO) on March 11, 2020 (Lai et al., 2020). As of October 28, 2022, there have been over 629 million confirmed cases of COVID-19 worldwide, with a total of more than 6 million deaths (WHO, 2022). In Indonesia, as of November 12, 2022, more than 6 million patients tested positive with more than 159,000 deaths (Ministry of Health, 2022). SARS-CoV-2 is composed of positive single-stranded RNA with the largest genome structure (26.4-31.7 kb) among all known RNA viruses (Mousavizadeh, & Ghasemi, 2021). The genome encodes four structural proteins, including spike (S), membrane (M), envelope (E), and nucleocapsid (N) as well as 16 non-structural proteins (nsp) (Boopathi et al., 2020). Among these 16 nsp, two are proteases, and one of them is Papain-Like protease (PLpro).

PLpro is an essential enzyme that is involved in several critical processes of the viral replication cycle. Furthermore, it can process viral polyproteins by recognizing LXGG cutting motifs that cut the bonds between nsp1-nsp2, nsp2-nsp3, and nsp3-nsp4 to produce nsp1, nsp2, and nsp3 (Armstrong et al., 2021). PLpro also plays a role in the cleavage and maturation of polyproteins, the formation of replicate-transcriptase complexes, as well as the breaking of bonds in the ubiquitin and Interferon-Stimulated Gene 15 (ISG15) chains that signal the host's innate immune response to viral infections (Klemm et al., 2020). Its inhibition can prevent viral replication and dysregulation of the host's immune system, making it an effective therapeutic agent for COVID-19 (Osipiuk et al., 2021).

Several medicinal plants have been reported to be potential sources of natural antiviral compounds (Attia et al., 2020). Among these plants are bay leaf *(Syzygium polyanthum)*, mahogany bark *(Swietenia macrophylla)*, and white teak bark (*Gmelina arborea* Roxb.). Flavonoid is the main component of bay leaf and mahogany bark (Novira, & Febrina, 2018). The compound is known to provide several benefits,

including antivirals, antibacterials, antifungals, anti-inflammatory, and antioxidants. In silico studies also showed that it has inhibitory activity against several target proteins in SARS-CoV-2, such as the enzyme main protease (Mpro), RNA-dependent RNA polymerase (RdRp), and spike (Alzaabi et al., 2022; Bharathi et al., 2022). Meanwhile, white teak bark has been found to exhibit weak to moderate antioxidant activity. Several studies also reported that antivirals and antioxidants have a close relationship, as viral infections are often accompanied by oxidative stress, a key factor in viral pathogenesis (Fedoreyev et al., 2018).

At present, there are no studies on the potential of flavonoid compounds from bay leaf and mahogany bark, as well as phenolic compounds from white teak bark, as PLpro SARS-CoV-2 inhibitors. Therefore, this study aims to investigate the ability of these compounds to inhibit PLpro SARS-CoV-2.

EXPERIMENTAL SECTION

The materials used in this study consisted of a 3D PLpro structure (PDB ID: 6wx4) downloaded from the RCSB online database https://www.rcsb.org/ in *.pdb format as well as reference, and test ligands from PubChem online database https://pubchem.ncbi.nlm.nih.gov/. The reference ligands included benserazide and ribavirin. Meanwhile, the test ligands were flavonoid compounds derived from bay leaf and mahogany bark, and phenolic compounds from white teak bark (Appendix 1).

Conserved Amino Acid Analysis (Kakar et al., 2021)

The 3D receptor structure in *.pdb format was uploaded to the Consurf webserver (https://consurf.tau.ac.il/index_proteins.php) for analysis of conserved amino acids. Furthermore, the analysis results were in the form of amino acid sequences and 3D structure of receptors with color labels based on the level of conservation.

Analysis of Druggability (Volkamer Modification et al., 2012).

The potential of a pocket in binding to drug compounds was predicted using the webserver DoGSiteScorer (https://proteins.plus/#dogsite). The output was then presented as a table with the best pocket information and visualizations in the form of 3D images.

Preparation of Receptor and Native Ligand Structures (Siagian Modification et al., 2022)

The 3D structure of receptors in the *.pdb format was prepared using YASARA (Krieger et al., 2009), including the removal of water and residues, the addition of hydrogen, as well as the separation of the receptors and native ligand. The preparation results were presented in *.mol2 format and consisted of receptor structures with coenzymes (Zn) but without native ligand, as well as native ligand without receptors and coenzymes. The products were then prepared using Marvin Sketch with conditioning at a pH of 7.4 with 20 conformations. Subsequently, the conformation file was saved in the *.mol2 format.

Validation of Molecular Docking (Siagian Modifications et al., 2022)

Molecular docking was validated by redocking native ligand (VIR251) to receptors using PLANTS. After obtaining the docking score, the Root Mean Square Deviation (RMSD) value was calculated using the YASARA structure.

Preparation of Ligands and Molecular Docking (Siagian Modification et al., 2022)

The test and reference ligands were prepared by Marvin Sketch, and then conditioned at a pH of 7.4 to form 20 kinds of conformations. Subsequently, molecular docking was carried out using PLANTS. The docking results with the most negative binding affinity scores were selected for analysis and visualization.

Visualization of Molecular Docking (Siagian Modifications et al., 2022)

The docking ligands in the *.mol2 format were converted into *.pdb using YASARA structure and attached to receptors using Discovery Studio Client 2016 (Pilot, 2016). Visualization was then carried out in two and three dimensions using LigPlot+ 1.5.4 (Lakowski et al., 2011) and PyMOL (Yuan et al., 2017), respectively, with an interaction radius of 5Å from the docked ligand position.

Prediction of Physicochemical, Pharmacokinetic, and Ligands Toxicity (Modification of Hamzah et al., 2015)

Physicochemical predictions of ligands were performed using the Lipinski webserver (http://www.scfbio-iitd.res.in/ software/drugdesign/lipinski.jsp) by inputting their files in *.pdb format. Meanwhile, pharmacokinetic predictions were carried out by inputting smiles from ligands on the SwissADME webserver (http://www.swissadme.ch/) and pkCSM online tool (http://biosig.unimelb.edu.au/pkcsm/prediction). Toxicity predictions were carried out on the AdmetSAR (http://lmmd.ecust.edu.cn/admetsar1/predict/) webserver.

RESULTS AND DISCUSSION

Conserved Amino Acid Analysis

The identification of conserved amino acids was carried out by estimating the conservation of the evolution of amino acid positions in protein molecules based on phylogenetic relationships between homologous sequences (Ashkenazy et al., 2016). The analysis results showed that the ligand was on the binding pocket receptor, as shown in **Figure 1a**. Furthermore, the binding pocket was composed of catalytic residues Cys111, His272, and Asp286, as well as substrate binding sites on Thr106, Asn109, Leu162, Gly163, Asp164, Arg 166, Met208, Pro247, Pro248, Tyr264, Tyr268, Gln269, Cys270, Gly271, Tyr273 and Thr301 (Rut et al., 2020; Osipiuk et al., 2021). Based on the identification results, the catalytic

residues were conservative, as indicated by the red color, while the constituent residues of the substrate binding side were variable to conservative and shown with green to red (**Figure 1b**). Kakar et al., (2021) reported that conservative residues played an important role in protein activity.

Drugability Analysis

The analysis results of a pocket's ability to interact with medicinal compounds were taken from five samples with the best drug score. Pockets 1 to 5 had varying values of volume, surface area, depth, and hydrophobicity, while the drug score showed a decreasing trend, as shown in **Table 1**. Volkamer et al., (2012) reported that large volumes and depths and high hydrophobicity values are important parameters in determining drugability. Furthermore, drugability was determined based on the drug score with a range of 0 (undruggable) to 1 (druggable). Pocket 1 had the largest volume, surface area, and druggability value, but its depth and hydrophobicity were not greater than 2 and 3. It also had an active site containing catalytic sites from receptors as well as a spot for native ligand (VIR251) binding, as shown in **Figure 2**. Pocket 1 was used as a docking target in this study based on these results.

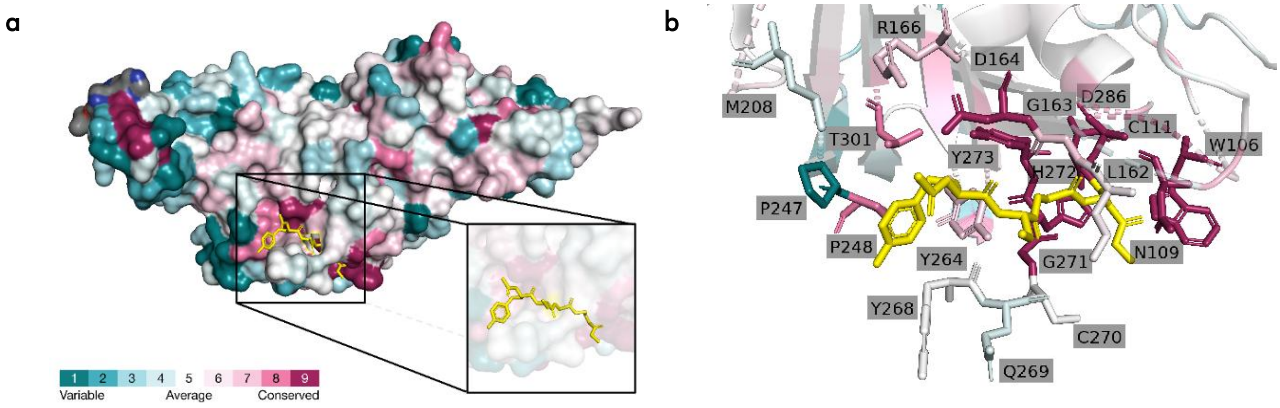

Figure 1. Visualization results of the identification of conserved residues. (a) binding pocket receptors, and (b) catalytic residues as well as substrate binding residues. The yellow stick structures a native ligand of VIR251

Table 1. Pocket data 6wx4 DoGSiteScorer prediction results

Name	Volume (A^3)	Surface Area ($Å^2$)	Depth (Z)	Hydrophobicity	Drug Score
Pocket 1	404.86	631.70	16.28	0.40	0.70
Pocket 2	313.92	602.13	14.63	0.43	0.63
Pocket 3	205.18	482.81	16.68	0.30	0.62
Pocket 4	201.66	409.92	15.33	0.38	0.59
Pocket 5	333.70	504.56	12.58	0.18	0.57

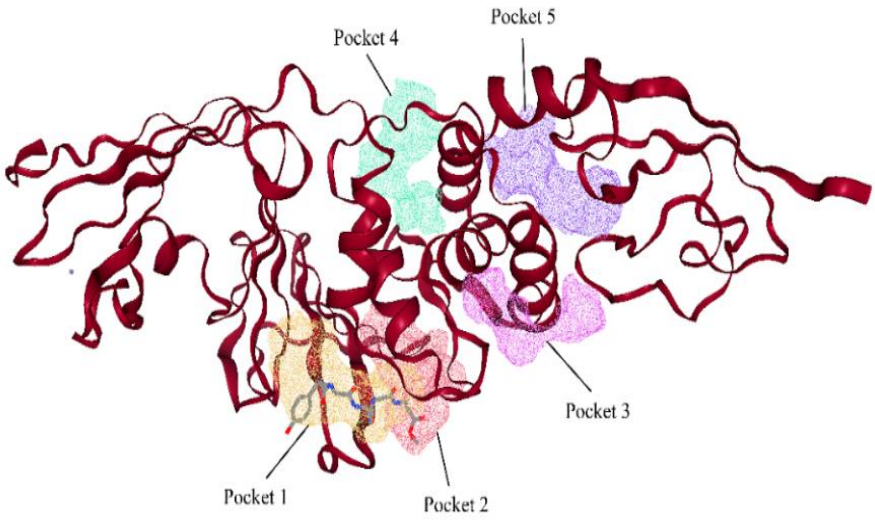

Figure 2. DoGSiteScorer's predicted 6wx4 pocket visualization

Validation of Receptor and Molecular Docking

Molecular docking was carried out by predicting the structure of intermolecular complex ligands and receptors expressed in the bond-free energy as well as the type of interaction (Sumaryada, 2016). Furthermore, validation was performed against the docking method before the simulation. The process was carried out on binding site centers 9.30159, -27.689, and -37.813 with a radius of 14.7701. RMSD value parameters were then used to assess 20 native ligand conformations (VIR251) with 10 repetitions per conformation. The validation results obtained an RMSD value of 1.2255 Å (Appendix 2) with the redocking ligand pose closely resembling that of the native ligand, as shown in **Figure 3**. According to Pratama et al., (2021), an RMSD value of < 2 Å indicated that the docking method was valid and can be used for subsequent processes.

Docking was performed on 11 bay leaf, 3 mahogany bark, and 6 white teak bark test ligands (Appendix 1). The results were then compared with VIR251 as a native ligand, as well as benserazide and ribavirin as references. Benserazide was selected due to its high potential to bind to PLpro SARS-CoV-2 through hydrogen bonds in the residues of Asp164 and Gln269. It can also engage in hydrophobic binding to Tyr268, Pro247, and Pro248 (Ibrahim et al., 2020). Meanwhile, ribavirin was recommended for emergency use as an antiviral agent for SARS-CoV-2. Molecular docking studies showed that it can inhibit the activity of PLpro enzyme by binding to the substrate binding site of Gln270 (Wu et al., 2020). The docking results were selected based on the samples with the highest negative binding energy (ΔG) value.

Furthermore, VIR251 had the highest negative bond energy value of -115.54 kcal/mol compared to the overall test ligands, as well as benserazide and ribavirin with s-90.93 kcal/mol and -74.06 kcal/mol, respectively (**Table 2**). This was because VIR251 was a nonproteinogenic peptide that can selectively inhibit PLpro SARS-CoV-2 (Rut et al., 2020). Several test ligands were also reported to have higher negative binding energy values compared to the references. Quercitrin, myricitrin, epigallocatechin-3-gallate, and myricetin from bay leaf, as well as the overall test ligand from mahogany bark, had higher values compared to ribavirin. Similar findings were also obtained from balanophonin, gmelinol, and (−)-p-hydroxyphenyletil[5‴-O-(3,4-dimetoxysinamoyl)-β-D-apiofuranosil(1‴ → 6′)]-β-D-glucopyranose from white teak bark, which had more negative binding energy. However, only epigallocatechin-3-gallate from bay leaf, swietemacrophyllanin from mahogany bark, as well as (−)-p-hydroxyphenyletil[5‴-O-(3,4-dimetoxysinamoyl)-β-D-apiofuranosil(1‴ → 6′)]-β-D-glucopyranose from white teak bark had higher energy value compared to benserazide (**Table 2**). A high negative binding energy (ΔG) indicated the presence of a high ligand affinity to the active site of the receptors as well as strong ligand-receptor bonds (Pratama, & Suhartono, 2018).

Prediction of Physicochemical Properties, Pharmacokinetics, and Ligand Toxicity

Test ligands with a higher binding energy value were analyzed using the prediction of physicochemical properties, pharmacokinetics, and toxicity. Furthermore, the physicochemical characteristics are one of the factors that must be considered in the design of a drug. One of the indicators used in this study was the Lipinski Rule of Five. Lipinski et al., (2001) reported that a compound has good absorption and permeation when the relative atomic mass, hydrogen bond donor, bond acceptor, partition coefficient (Log P), and molar refractivity of < 500 Da, < 5, < 10, < 5, and 40-130, respectively. A ligand is believed to meet Lipinski's rule when it does not violate more than 2 parameters (Petit et al., 2012). Based on the results of the analysis, all reference and test ligands met the rule except for (−)-p-hydroxypheniletil[5‴-O-(3,4-dimethoxysinamoyl)-β-D-apiofuranosil (1‴→6′)]-β-D-glucopyranoside. This was because it violated 4 test parameters, as shown in **Table 3**. Drugs that do not meet the Lipinski Rule of Five were likely to cause problems during oral usage, hence, the molecules were often administered using intravenous injection (Amirian, & Levy, 2020).

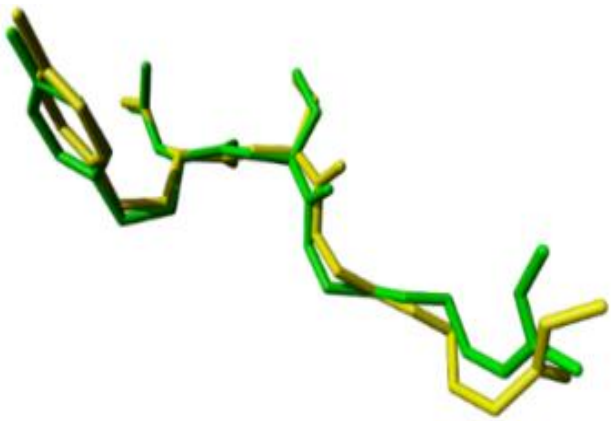

Figure 3. Validated ligand pose (green) with crystallographic data (yellow)

Table 2. Ligands molecular docking score against PLpro SARS-CoV-2 6wx4

Ligands	Binding Energy (kcal/mol)
VIR251 (native ligand)	-115.54
Benserazide (reference ligand)	-90.93
Ribavirin (reference ligand)	-74.06
S. polyanthum leaf	
Quercitrin	-81.82
Myricitrin	-83.97
Epigallocatechin-3-gallate	-98.93
Myricetin	-74.22
Quercetagetin	-73.80
Quercetin	-73.13
Malvidin	-71.58
Delphinidin	-73.92
Phloretin	-73.02
Retusin	-67.67
Flavan-3-ol	-71.08
S. macrophylla bark	
Catechin	-80.10
Epicatechin	-80.12
Swietemacrophyllanin	-91.22
G. arborea bark	
Balanophonin	-83.36
Gmelinol	-87.94
(−)-p-hydroxyphenylethyl[5‴-O-(3,4-dimethoxysinamoyl)-β-D-apiofuranocyl(1‴ → 6′)]-β-D-glucopyranoside	-107.78
2-(4-hydroxyphenyl) ethanol	-60.48
2,6-dimethoxy-p-benzoquinone	-58.29
3,4,5-trimethoxyphenol	-59.68

Description: The yellow line is a test ligand with a binding energy that exceeds the reference ligand

Table 3. Prediction of ligands' physicochemical properties

Ligands	Relative Atom Mass (Da)	Hydrogen Bond Donor	Hydrogen Bond Acceptor	LogP	Molar Refractivity
VIR251 (Native ligand)	477.00	6.00	7.00	2.19	117.10
Benserazid (Reference ligand)	258.00	6.00	8.00	-1.07	56.93
Ribavarin (Reference ligand)	244.00	5.00	8.00	-3.01	51.55
S. polyanthum leaf					
Quercitrin	448.38	7.00	11.00	0.49	109.00
Myricitrin	464.38	8.00	12.00	0.19	111.02
Epigallocatechinn-3-gallate	458.38	8.00	11.00	2.23	112.06
Myricetin	318.24	6.00	6.00	1.69	80.06
S. macrophylla bark					
Catechins	290.00	5.00	6.00	1.09	68.13
Epicatechin	290.00	5.00	6.00	1.09	68.13
Swietemakrofilanin	482.00	6.00	10.00	2.04	110.90
G. arborea Roxb. bark					
Balanophonin	356.00	2.00	6.00	2.83	95.95
Gmelinol	402.00	1.00	7.00	2.91	104.92
(−)-p-hydroxyphenylethyl[5‴-O-(3,4-dimetoxysinamoyl)-β-D-apiofuranosil(1‴ → 6′)]-β-D-glucopyranoside	622.00	6.00	14.00	-0.50	150.63

Description: yellow box = breaking Lipinski's rules

Prediction of ligand pharmacokinetics must be carried out to determine the absorption, distribution, metabolism, and excretory power of the compounds to be developed into drugs (Novian et al., 2019). The analysis was based on several parameters, including %absorption, water solubility, gastrointestinal absorption (GI), Log Kp (skin permeability), and bioavailability. Furthermore, absorption was a parameter used to predict the proportion of compounds absorbed through the human small intestine. The analysis results showed that the overall reference and test ligands had an absorption value of 36-96%, while a value of 25.82% was obtained from the native variants, as shown in **Table 4**. This indicated that the reference and test ligands were well absorbed because they have an absorption value of >30% (Pires et al., 2015). Water solubility was one of the parameters used to predict the absorption of drugs in the body. Daina et al., (2017) reported that the injected drug candidate must be water-soluble. The results showed that the two reference ligands were highly soluble in water, while all test and native ligand had water-soluble properties. However, only swietemacrophyllanin from mahogany bark was slightly soluble in water, as shown in **Table 4**.

Prediction of drug absorption through diffusion in the human gastrointestinal tract showed that all samples from bay leaf as well as swietemacrophyllanin from *S. macrophylla* bark, and (−)-p-hydroxypheniletil[5‴-O-(3,4-dimetoxysinamoyl) -β-D-apiofuranosil(1‴→6′)]β-D-glucopyranosee from *G. arborea* bark had a low GI absorption rate. Meanwhile, the two test ligands from *Swietenia macrophylla* bark and *G. arborea*, namely catechin, epicatechin, balanophonin, and gmelinol had higher values, as shown in **Table 4**. According to Daina et al., (2017), compounds with a good pharmacokinetic profile were determined by high GI absorption. The skin permeability parameter (Log Kp) played an important role in drug delivery. Compounds with low skin permeability are characterized by a Log Kp value of >-2.5 (Pires et al., 2015). Based on the analysis results, native, reference, and test ligands have a permeability value of < -2.5, indicating good skin permeability, as shown in **Table 4**. Meanwhile, the bioavailability prediction was carried out by measuring the dose of the drug administered that reached the systemic circulation (McGinnity, & Grime, 2017). The bioavailability score was categorized as good when the value obtained was > 0.10 (Daina et al., 2017). The prediction results showed that all ligands have scores of > 10% or 0.10, as shown in **Table 4**. This indicates that they can be used as effective alternative therapies.

Another crucial aspect of drug design is toxicity prediction, which played an important role in estimating the degree of damage caused by compounds to biological and nonbiological materials. It can also be used to assess the risk of cancer, heart disorders, and skin or eye irritation (Sasmito et al., 2015). Predictions were made based on three parameters, including Human Ether-a-go-go-Related gene (hERG) inhibition, carcinogenicity, and acute oral toxicity. Furthermore, hERG encoded the pore-forming

Table 4. Ligand pharmacokinetic prediction

Ligands	Absorption (%)	Water solubility	GI Absorption	Log kp (cm/s)	Bioavailability score
VIR251 (Native ligand)	25.82	Soluble	Low	-10.06	0.17
Benserazid (Reference ligand)	36.00	Very soluble	Low	-8.77	0.55
Ribavarin (Reference ligand)	54.99	Very soluble	Low	-9.10	0.55
S. polyanthum leaf					
Quercitrin	52.71	Soluble	Low	-8.42	0.17
Myricitrin	43.33	Soluble	Low	-8.77	0.17
Epigallocatechinn-3-gallate	47.40	Soluble	Low	-8.27	0.17
Myricetin	62.82	Soluble	Low	-7.40	0.55
S. macrophylla bark					
Catechins	68.83	Soluble	High	-7.82	0.55
Epicatechin	68.83	Soluble	High	-7.82	0.55
Swietemakrofilanin	83.99	Slightly Soluble	Low	-7.67	0.55
G. arborea Roxb. Bark					
Balanophonin	96.00	Soluble	High	-7.03	0.55
Gmelinol	95.00	Soluble	High	-7.42	0.55
(−)-p-hydroksiphenylethyl[5‴-O-(3,4-dimetoxysinamoil)-β-D-apiofuranosil(1‴ →6′)]-β-D-glucopyranoside	36.00	Soluble	Low	-10.23	0.17

subunits of the K+ ion channels in the heart that played a role in electrophysiology. This indicates that inhibition of the gene can increase the probability of arrhythmias and sudden death (Lei et al., 2019; Dickson et al., 2020). The analysis results showed that native ligand, swietemacrophyllanin from *S. macrophylla* bark, and gmelinol from *G. arborea* bark inhibited hERG with a probability of greater than 0.50. This indicated that the three ligands cannot be used as drug candidates. Meanwhile, the test ligand, epigallocatechin-3-gallate from *S. polyanthum* leaf, inhibits hERG with a probability of less than 0.50, indicating a low level of hERG inhibition (**Table 5**).

A carcinogenic parameter helped to reveal the nature of a compound with the ability to cause cancer by damaging DNA and disrupting the body's biological processes (Arief et al., 2018). Based on the analysis results, native, test, and reference ligands were non-carcinogenic, indicating they were safe, as shown in **Table 5**. Meanwhile, an acute oral toxicity test parameter was performed to determine the LD_{50} value of a compound. The Lethal Dose 50 (LD 50) value was a dose that statically has the ability to kill 50% of the experimental target (Sulastra et al., 2020). Acute oral toxicity was divided into four categories based on the United States Environmental Protection Agency. The categories included I, II, III, and IV with LD values of 50 ≤ 50 mg/kg, 50 < LD 50 ≤ 500 mg/kg, 500 < LD 50 ≤ 5000 mg/kg, and 50 ≥ 5000 mg/kg, respectively (Gadaleta et al., 2019). Based on the results, all the ligands were in category III. The only exceptions were myricetin in II, as well as epigallocatechin-3-gallate from *S. polyanthum* leaf and catechins and epicatechin from *S. macrophylla* bark in IV. This showed that all the compounds were considered to have relatively low toxicity, except for the myricetin test ligand from *S. polyanthum* leaf, as shown in **Table 5**.

Epigallocatechin-3-gallate from *S. polyanthum* leaf, catechins and epicatechins from *S. macrophylla* bark, and balanophonins from *G. arborea* bark had the best characteristics based on these predictions. This indicated that they can be used to develop effective alternative medicine for SARS-CoV2. However, these compounds have low GI absorption values, which reduced their effectiveness. VIR251 (native ligand) has a small absorption value and can inhibit hERG with a probability of 0.75. Based on this finding, it was predicted that the body can experience difficulties during its absorption, leading to increased arrhythmias and sudden death.

Analysis and Visualization of Molecular Docking

Analysis and visualization were performed on test ligands with a docking score that was more negative compared to the reference. Visualization was carried out in 2D (Appendix 3) and 3D (**Figure 4**). The 2D process was performed to analyze the binding interaction of receptor complexes with VIR251, as well as the reference and test ligands, as shown in **Table 6**. Meanwhile, 3D visualization was carried out to analyze ligand poses on the binding pocket, as shown in **Figure 4**. The analysis was based on the reports of Rut et al., (2020) & Osipiuk et al., (2021) that PLpro SARS-CoV-2 has catalytic sites on the Cys111, His272, and Asp286 residues. It also has substrate binding sites on the Thr106, Asn109, Leu162, Gly163, Asp164, Arg 166, Met208, Pro247, Pro248, Tyr264, Tyr268, Gln269, Cys270, Gly271, Tyr273, and Thr301 residues.

Table 5. Ligands Toxicity Prediction

Ligands	hERG		Carcinogenicity		Acute oral toxicity	
	Category	Score	Category	Score	Category	Score
VIR251 (Native ligand)	+	0.75	Non-carcinogens	0.92	III	0.68
Benserazid (Reference ligand)	-	0.99	Non-carcinogens	0.76	III	0.74
Ribavirin (Reference ligand)	-	0.64	Non-carcinogens	0.99	III	0.78
S. polyanthum leaf						
Quercitrin	-	0.98	Non-carcinogens	0.95	III	0.52
Myricitrin	-	0.59	Non-carcinogens	0.99	III	0.52
Epigallocatechinn-3-gallate	+	0.14	Non-carcinogens	0.96	IV	0.38
Myricetin	-	0.78	Non-carcinogens	1.00	II	0.73
S. macrophylla bark						
Catechins	-	0.47	Non-carcinogens	0.97	IV	0.64
Epicatechin	-	0.47	Non-carcinogens	0.97	IV	0.64
Swietemakrofilanin	+	0.87	Non-carcinogens	0.99	III	0.65
G. arborea bark						
Balanophonin	-	0.97	Non-carcinogens	0.91	III	0.57
Gmelinol	+	0.70	Non-carcinogens	0.90	III	0.48
(−)-p-hydroksiphenylethyl[5‴-O-(3,4-dimethoxysinamoil)-β-D-apiofuranosil(1‴ → 6′)]-β-D-glucopyranoside	-	0.47	Non-carcinogens	0.97	III	0.55

Based on the analysis results, only native ligand interacted with the catalytic site of the receptor, while the reference and test ligands were only associated with the substrate binding site (**Table 6**). These results were also observed in 3D visualization of the binding pocket. The native ligand on the binding pocket at the catalytic site was yellow, while the reference and test ligands on the substrate binding pocket were blue (Figure 4). This occurred because the pocket in the catalytic part of PLpro SARS-CoV-2 had a very narrow geometric structure, thereby requiring a very flexible compound (Narayanan et al., 2022).

The docking results also showed the multiplicity of hydrophobic interactions as well as hydrogen bonds in each ligand, as shown in **Table 6**. The difference in the number of hydrophobic interactions was because the number of amino acids with nonpolar side chains at the receptor was lesser compared to the polar side chains (Zhu et al., 2016). According to Arwansyah et al., (2014), the abundance of hydrophobic interactions played a role in determining the stability of ligands tethered to receptors. Meanwhile, the difference in the number of hydrogen bonds was likely due to variations in the amount of hydrogen bond donors and acceptors in each compound (Chen et al., 2016). Due to the numerous hydrogen bonds, the ΔG value was more negative, thereby strengthening the ligand and receptor bonds (Tallei et al., (2020); Alimah et al., (2022)). The analysis results showed that benzeradine had the highest number of hydrogen bonds, but the resulting ΔG value was lower compared to the native ligand. This was because the native ligand bonded to catalytic sites that played an important role in the enzymatic reactions of receptors (**Table 3**). Epigallocatechin-3-gallate, swietemacrophyllanin, and (−)- p-hydroxypheniletil[5‴-O-(3,4-dimethoxysinamoyl)-β-D-apiofuranosil(1‴ → 6′)]-β-D-glucopyranose had the highest number of hydrogen bonds among the compounds obtained from the plant used (**Table 6**). These results correlated to the ΔG value of the three ligands, which had the highest ΔG value, as shown in **Table 2**. Furthermore, the distance of the hydrogen bond formed also influenced the interaction of ligands and receptors. According to Prasetiawati et al., (2021), these bindings were categorized as strong when they have a distance of < 2.8 Å. The (−)-p-hydroxyfeniletile[5‴-O-(3,4-dimethoxysinamoil)-β-D-apiofuranosil(1‴ → 6′)]-β-D-glucopyranose had 4 hydrogen bonds with a distance of < 2.8 Å, while native ligand had 3. The results also showed that the reference and other test ligands had 1-2 bonds.

Table 6. Residues involved in the binding complex

Ligands	Amino acid residues involved		The amount of residue involved	
	Hydrophobic interaction	Hydrogen bonding	Hydrophobic interaction	Hydrogen bonding
VIR251 (Native ligand)	Asn109, Asn110, Cys111, Leu162, Pro247, Pro248, Gln269, Cys270, Tyr273, Thr301	Trp106 (3.02 Å) Tyr112 (4.60 Å) Gly163 (2.60 and 3.08 Å) Asp164 (2.93 Å) Tyr264 (2.95 and 4.94 Å) Tyr268 (3.06 and 3.18 Å) Gly271 (2.77 and 2.79 Å) His272 (4.16 Å) Asp286 (2.98 Å)	10	13
Benserazid (Reference ligand)	Met208, Ser245, Pro247, Pro248	Asp164 (3.12 Å) Val165 (3.42 Å) Arg166 (2.89, 2.92, and 3.91 Å) Ala246 (3.84 and 3.92 Å) Tyr264 (2.86 and 4.96 Å) Tyr267 (4.82 Å) Tyr268 (2.95 Å) Tyr273 (2.79 Å) Thr301 (2.87, 2.87, 2.99, and 4.98 Å) Asp302 (2.59 and 3.00 Å)	4	18
Ribavirin (Reference ligand)	ASP164, GLU167, PRO247, PRO248, GLN269	Lys157 (3.87 Å) Leu162 (3.01 Å) Gly163 (2.85 and 3.61 Å) Tyr264 (4.04 and 4.94 Å) Tyr268 (2.75 and 4.77 Å) Tyr273 (2.99 Å) Thr301 (3.02 and 3.16 Å)	5	11

S. polyanthum leaf				
Quercitrin	Asp164, Met208, Ala246, Pro247, Asn267	Gly163 (4.97 Å) Val165 (4.91 Å) Arg166 (4.83 and 4.83 Å) Pro248 (4.04 Å) Tyr264 (4.25 Å) Gly266 (2.69 Å) Tyr268 (3.59 Å) Tyr273 (2.76 and 3.25 Å) Thr301 (4.85 Å) Asp302 (4.98 Å)	5	12
Myricitrin	Gly163, Pro247, Pro248, Thr265, Asn267, Thr301	Asp164 (4.70 Å) Val165 (4.91 Å) Tyr264 (3.92 and 4.30 Å) Gly266 (2.71 and 2.91 Å) Tyr268 (3.07 and 3.71 Å) Tyr273 (2.95 Å)	6	9
Epigallocatechin-3-gallate	Asp164, Met208, Pro247, Pro248	Gly163 (3.48 and 4.82 Å) Val165 (4.83 and 4.92 Å) Arg166 (2.85, 2.99, 3.00, and 3.59 Å) Tyr264 (2.86 and 4.93 Å) Gly266 (4.17 Å) Asn267 (4.90 Å) Tyr268 (2.91 Å) Tyr273 (2.62 and 2.94 Å) Thr301 (3.80 Å)	4	16
Myricetin	Pro247, Pro248, Asn267	Gly163 (4.69 Å) Asp164 (2.47, 2.92, 4.85 Å) Val165 (4.47 Å) Tyr264 (4.45 Å) Gly266 (2.92 Å) Tyr268 (4.90 Å) Tyr273 (2.48 and 2.97 Å) Thr301 (3.05 Å)	3	11
S. macrophylla bark				
Catechin	Pro247, Pro248, Asn267, Tyr268	Gly163 (4.01 Å) Asp164 (4.10 Å) Val165 (4.78 Å) Tyr264 (4.81 Å) Gly266 (2.97 Å) Tyr273 (2.67 and 2.96 Å) Thr301 (3.08 Å)	4	8
Epicatechin	Pro247, Pro248, Asn267, Tyr268	Gly163 (4.00 Å) Asp164 (4.03 Å) Val165 (4.71 Å) Tyr264 (4.80 Å) Gly266 (2.98 Å) Tyr273 (2.62 and 2.95 Å) Thr301 (3.05 Å)	4	8
Swietemakrophyllanin	Gly163, Met208, Ser245, Pro247, Ala249, Thr265, Asn267, Tyr273, Pro299	Asp164 (4.17 Å) Arg166 (3.01,3.39, and 4.08 Å) Ala246 (3.93 and 4.71 Å) Pro248 (4.99 Å) Tyr264 (3.20 Å) Gly266 (2.53 and 4.96 Å) Tyr268 (2.97 Å) Thr301 (3.04 and 4.40 Å) Asp302 (4.55 Å)	9	14

		G. arborea Roxb. bark		
Balanophonin	Asp164, Pro247, Pro248, Thr265, Asn267, Tyr268, Thr301	Tyr264 (4.24 and 4.31 Å) Gly266 (2.66 Å) Tyr273 (2.84 Å)	7	4
Gmelinol	Leu162, Gly163, Pro247, Pro248, Gly266, Asn267, Tyr268, Gln269, Cys270, Gly271, Thr301	Asp164 (2.69 Å) Tyr264 (2.88 and 4.37 Å) Tyr273 (2.75 Å)	11	4
(−)-p-hydroksiphenylethyl[5‴-O-(3,4-dimetoxysinamoyl)-β-D-apiofuranosil(1‴ → 6′)]-β-D-glucopyranoside	Asn109, Gly160, Asp164, Pro247, Pro248, Gly266, Asn267, Tyr268, Gln269	Lys157 (3.06 Å) Val159 (4.79 Å) Glu161 (2.51 and 2.96 Å) Leu162 (2.77, 4.00, and 4.93 Å) Gly163 (2.42, 2.69, and 3.33 Å) Val165 (4.96 Å) Tyr264 (4.24 Å) Tyr273 (3.24 and 4.82 Å)	9	8

Description: The residue given yellow color is the catalytic site of the enzyme while the residue given blue is the substrate binding site.

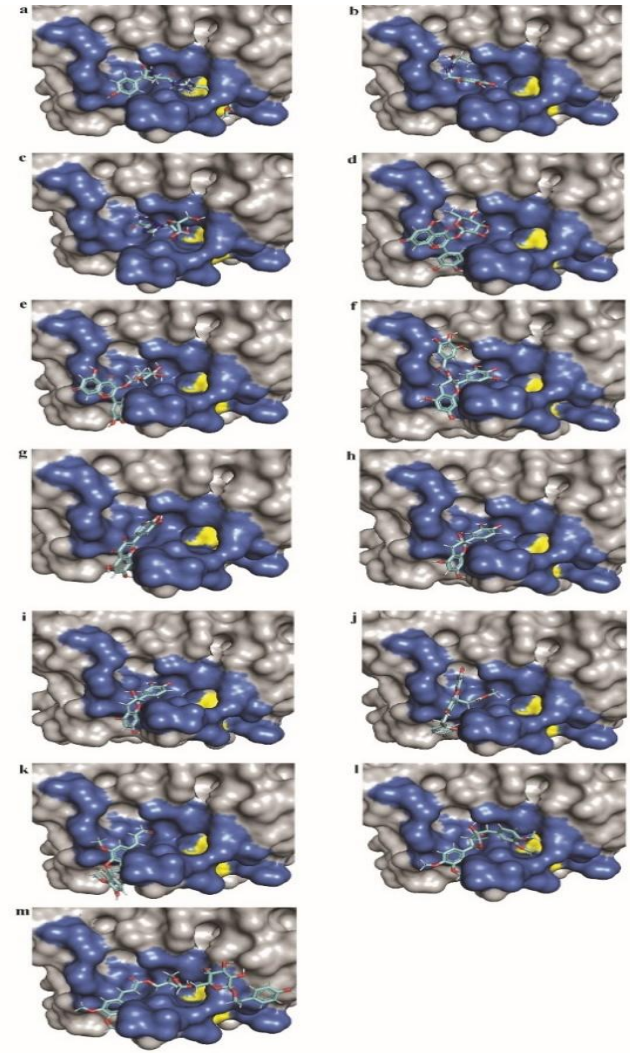

Figure 4. Visualization of 3D binding pocket PLpro SARS-CoV-2 with (**a**) native ligand VIR251, (**b**) Benserazide, (**c**) Ribavirin, (**d**) Quercitrin, (**e**) Myricitrin, (**f**) Epigallocatechin-3-gallate, (**g**) Myricetin, (**h**) Catechin, (**i**) Epicatechin, (**j**) Swietemacrophyllanin, (k) Balanophonin (**l**) Gmelinol, (m) (−)-p-hydroxyphenyletil[5‴-O-(3,4-dimethoxysinamoyl)-β-D-apiofuranosil (1‴ → 6′)]-β-D-glucopyranoside.

CONCLUSIONS

The test ligands epigallocatechin-3-gallate (-98.93 kcal/mol) from *S. polyanthum* leaves, catechin (-80.10 kcal/mol) and epicatechin (-80.12 kcal/mol) from *S. macrophylla* bark, and balanophonin (-83.36 kcal/mol) from *G. arborea* bark were the best test ligands based on binding energy compared to the reference ligands ribavirin (-74.06 kcal/mol) and benserazide (-90.93 kcal/mol). Additionally, these four ligands met the predictions for pharmacokinetic, physicochemical, and toxicity tests, in contrast to the natural ligand VIR251, which showed a 75% probability of hERG inhibition. This indicates that the test ligands epigallocatechin-3-gallate, catechins, epicatechins, and balanophonins demonstrated the most promising drug-like properties, suggesting their potential as alternative antiviral agents against SARS-CoV-2.

REFERENCES

Alimah, S. N., Sumaryada, T. I., Nurcholis, W., & Ambarsari, L. (2022). Molecular docking study of IPBCC.08.610 glucose oxidase mutant for increasing gluconic acid production: *Jurnal Kimia Sains dan Aplikasi, 25*(5), 169-178.

Alwie, R., R., Mumpuni, E., Sulastri, L., & Simanjuntak, P. (2021). Activity of *Syzygium polyanthum* leaf ethanol extract [*Syzygium polyanthum* (Wight) Walp.] as an inhibitor of the enzyme α-glucosidase and in *silico* studies: *Journal Phytopharmaceuticals, 8* (v2), 36 42.

Alzaabi, M. M., Hamdy, R., Ashmawy, N. S., Hamoda, A., M., Alkhayat, F., Khademi, N., N., Al-Joud, S. M. A., El-Keblawy, A. A., & Soliman, S. S. M. (2022). Flavonoids are promising safe therapy against COVID-19: *Phytochemistry Reviews*, *21*, 291-312.

Amirian, E. S., & Levy, J. K. (2020). Current knowledge about the antivirals remdesivir (GS-5734) and GS-441524 as herapeutic options for coronaviruses: *One Health, 9*, 1-7.

Arief, A., Bialangi, M. S., & Tureni, D. (2018). The level of knowledge about the dangers of smoking in students of SMP Negeri 15 Palu: *Journal of Biological Science and Education, 6*(2), 358-363.

Armstrong, L. A., Lange, S., M., Cesare, V., D., Matthews, S. P., Nirujogi, R. S., Cole, I., Hope, A., Cunningham, F., Toth, R., & Mukherjee, R. (2021). Biochemical characterization of protease activity of Nsp3 from SARS-CoV-2 and its inhibition by nanobodies: *PLoS ONE, 16*(7), 1-25.

Arwansyah, Ambarsari, L., & Sumaryada, T., I. (2014). Simulasi docking senyawa kurkumin dan analognya sebagai inhibitor reseptor androgen pada kanker prostat: *Current Biomedicine, 1*(1), 11-19.

Ashkenazy, H., abadi, S., Martz, E., Chay, O., Mayrose, I., Pupko, T., & Ben-Tal, N. (2016). ConSurf 2016: An improved methodology to estimate and visualize evolutionary conservation in macromolecules: *Nucleic Acids Research, 44*, 344-350.

Attia, Y. A., Alagawany, M. M., Farag, M. R., Alkhatib, F. M., Khafaga, A. F., Abdel- Moneim, A. M. E., Asiry, K. A., Mesalam, N., M., Shafi, M. E., & Al-Harthi, M. A. (2020). Phytogenic products and phytochemicals as a candidate strategy to improve tolerance to coronavirus: *Frontiers in Veterinary Science, 7*, 1-18.

Bharathi, M., Sivamaruthi, B. S., Kesika, P., Thangaleela, S., & Chaiyasut, C. (2022). In silico screening of bioactive compounds of representative seaweeds to inhibit SARS-CoV-2 ACE2-bound omicron B.1.1.529 spike protein trimer: *Marine Drugs*, *20*(148), 1-18.

Boopathi, S., Poma, A. B., & Kolandaivelc, P. (2020). Novel 2019 coronavirus structure, mechanism of action, antiviral drug promises and rule out against its treatment: *Journal of Biomolecular Structure and Dynamics, 39*(9), 3409-3418.

Chen, D., Oezguen, N., Urvil, P., Ferguson, C., Dann, S. M., & Savidge, T. C. (2016). Regulation of protein-ligand binding affinity by hydrogen bond pairing: *Science Advances, 2*(3), 1-16.

Daina, A., Michielin, O., & Zoete, V. (2017). SwissADME: a free web tool to evaluate pharmacokinetics, drug-likeness and medicinal chemistry friendliness of small molecules: *Scientific Reports, 7*(42717), 1-13.

Dewijanti, I. D. (2020). Study of antidiabetic bioactivity and antioxidants of *Syzygium polyanthum* leaf extract (*Syzygium polyanthum* (Wight) Walp) [thesis]. Depok (ID): University of Indonesia.

Dickson, C., J., Vega, C., V., & Duca, J., S. (2020). Revealing molecular determinants of hERG blocker and activator binding: *Journal of Chemical Information and Modeling, 60*(1), 192-203.

Falah, S., Katayama, T., & Suzuki, T. (2008). Chemical constituents from *Gmelina arborea* bark and their antioxidant activity: *Journal of Wood Science, 54*(6), 483-489.

Falah, S., Suzuki, T., & Katayama, T. (2008). Chemical constituent from *Swietenia macrophylla* bark and their antioxidant activity: *Pakistan Journal of Biological Sciences, 11*(16), 23-40.

Fedoreyev, S. A., Krylova, N. V., Mishchenko, N. P., Vasileva, E. A., Pislyagin, E. A., Lunikhina, O., V., Lavrov, V. F., Svitich, O. A., Ebralidze, L. K., & Leonova, G. N. (2018). Antiviral and antioxidant properties of echinochrome A: *Marine Drugs, 16*(12), 509-519.

Gadaleta, D., Vukovic, K., Toma, C., Lavado, G., J., Karmaus, A., L., Mansouri, K., Kleinstreuer, N., C., Benfenati, E., & Roncaglioni, A. (2019). SAR

and QSAR modeling of a large collection of LD50 rat acute oral toxicity data: *Journal of Cheminformatics, 11*(58), 1-16.

Hamzah, N., Rauf, A., & Ariwanti. (2015). Study of the quantitative relationship of activity structure (HKSA) of 4-Aminoquinolin pyramidine-derived compounds, molecular docking, pharmacophore tracing, virtual screening, toxicity assays, and pharmacokinetic profiles as antimalarials in silico: *Jurnal Fitofarmaka Indonesia, 3*(4), 176-186.

Hasan, R., Lindarto, D., Siregar, G., A., & Mukhtar, Z. (2020). The effect of salam leaf (*Syzygium polyanthum* [Wight] Walp.) extract on inflammation in rat model of acute coronary syndrome: *Open Access Macedonian Journal of Medical Sciences, 8A*, 374-377.

Ibrahim, T., M., Ismail, M., I., Bauer, M., R., Bekhit, A., A., & Boeckler, F. M. (2020). Supporting SARS-CoV-2 *Papain-Like Protease* drug discovery: in silico methods and benchmarking: *Frontiers in Chemistry, 8*(592289), 1-17.

Kakar, M., U., Matloob, M., Dai, R., Deng, Y., Ullah, K., Kakar, I., U., Khaliq, G., Umer, M., Bhutto, Z., A., Fazlani, S., A., & Mehboob, M. Z. (2021). In silico screening and identification of deleterious missense SNPs along with their effects on CD-209 gene: An insight to CD-209 related diseases: *PLoS ONE, 16*(2), 1- 16.

Klemm, T., Ebert, G., Calleja, D., J., Allison, C., C., Richardson, L., W., Bernardini, J., P., Lu, B., G., C., Kuchel, N., W., Grohmann, C., & Shibata, Y. (2020). Mechanism and inhibition of the Papain-Like Protease, PLpro, of SARS-CoV-2: *The EMBO Journal, 39*(18), 1-17.

Krieger, E., Joo, K., Lee, J., Lee, J., Raman, S., Thompson, J., Tyka, M., Baker, D., & Karplus, K. (2009). Improving physical realism, stereochemistry, and side-chain accuracy in homology modeling: four approaches that performed well in CASP8: *Proteins: Structure, Function, and Bioinformatics, 77*, 114-122.

Lai, C., Shih, T, Ko W, Tang, H., & Hsuehe, P. (2020). severe acute respiratory syndrome coronavirus 2 (SARS-CoV-2) and coronavirus disease-2019 (COVID-19): The epidemic and the challenges. *International Journal of Antimicrobial Agents, 55*(3), 105924.

Laskowski, R., A., & Swindells, M. B. (2011). LigPlot+: multiple ligand-protein interaction diagrams for drug discovery. *Journal of Chemical Information and Modeling*, *51*(10), 2778-2786.

Lei, C. L., Clerx, M., Gavaghan, D. J., Polonchuk, L., Mirams, G., R., & Wang, K. (2019). Rapid characterization of hERG channel kinetics I: using an automated high-throughput system: *Biophysical Journal, 117*(12), 2438 – 2454.

Lipinski, C., A., Lombardo, F., Dominy, B., W., & Feeney, P., J. (2001). Experimental and computational approaches to estimate solubility and permeability in drug discovery and development settings: *Advanced Drug Delivery Reviews, 46*(1), 3-26.

McGinnity, D., F., & Grime, K. (2017). ADME optimization in drug discovery. In Chackalamannil S, Rotella D, Ward SE, editor. *Comprehensive Medicinal Chemistry III*. Amsterdam (NL): Elsevier. hlm 34–44.

Ministry of Health of the Republic of Indonesia. (2021). Spread of COVID-19 Cases in Indonesia. Accessed from https://infeksiemerging. kemkes.go.id/ dashboard/covid-19. [November 12, 2022]

Mousavizadeh, Leila, & Sorayya, G. (2021). Genotype and phenotype of COVID-19: Their roles in pathogenesis: *Journal of microbiology, immunology, and infection, 54*(2), 159-163.

Muthmainnah, N., A. (2016). Anti-inflammatory test of *Syzygium polyanthum* leaf ethanol extract (*Syzygium polyanthum*) by in vivo and in silico methods on quersitrin compounds [thesis]. Yogyakarta (ID): Muhammadiyah University of Yogyakarta.

Narayanan, A., Narwal, M., Majowicz, S., A., Varricchio, C., Toner, S., A., Ballatore, C., Brancale, A., Murakami, K. S., & Jose, J. (2022). Identification of SARS-CoV-2 inhibitors targeting Mpro and PLpro using in-cell-protease assay: *Communications Biology, 5*(169): 1-17.

Novian, D., R., Ikhwani, A., Z., N., & Winarso, A. (2019). Test pharmacodynamics, drug-likeness, pharmacokinetics and the interaction of the active compound snake wood *(Strychnos lucida)* as an inhibitor of *Plasmodium falciparum* in silico: *Nusantara Veterinary Journal, 2*(1), 70-78.

Novira, P., P., & Febrina, E. (2018). Review article: a review of the pharmacological activity of bay leaf extract (*Syzygium polyanthum* (Wight.) Walp): *Farmaka, 16*(2), 288-297.

Osipiuk, J., Azizi, S., A., Dvorkin, S., Endres, M., Jedrzejczak, R., Jones, K., A., Kang, S., Kathayat, R., S., Kim, Y., & Lisnyak, V., G. (2021). Structure of Papain-Like Protease from SARS-CoV-2 and its complexes with non-covalent inhibitors: *Nature Communications, 12*(743), 1-9.

Petit, J., Meurice, N., Kaiser, C., & Maggiora, G. (2012). Softening the rule of five-where to draw the line?: *Bioorganic & Medicinal Chemistry, 20*, 5343-5351.

Pilot, & Pipeline. (2016), Dassault Systèmes BIOVIA discovery studio modelling environment, In: Release.

Pires, D., E., V., Blundell, T., L., & Ascher, D., B. (2015). pkCSM: predicting small-molecule pharmacokinetic properties using graph-based signatures: *Journal of Medicinal Chemistry, 58*(9), 4066-4072.

Prasetiawati, R., Suherman, M., Permana, B., & Rahmawati. (2021). Molecular docking study of anthocyanidin compounds against Epidermal Growth Factor Receptor (EGFR) as anti-lung cancer*: Indonesian Journal of Pharmaceutical Science and Technology, 8*(1), 8-20.

Pratama, M., & Suhartono, E. (2018). Understanding the interaction between glutathione and acetaminophen: a docking study approach: *Dentino: Jurnal Kedokteran Gigi, 3*(2), 215-219.

Pratama, M., R., F., Poerwono, H., & Siswodihardjo, S. (2021). Introducing a two-dimensional graph of docking score difference vs. similarity of ligand-receptor interactions: *Indonesian Journal of Biotechnology, 26*(1), 54-60.

Rut, W., Lv, Z., Zmudzinski, M., Patchett, S., Nayak, D., Snipas, S., J., Oualid, F., E., Huang, T., T., Bekes, M., & Drag, M. (2020). Activity profiling and crystal structures of inhibitor-bound SARS-CoV-2 Papain-Like Protease: a framework for anti–COVID-19 drug design: *Science Advances, 6*(42), 1-12.

Sasmito, W., A., Wijayanti, A., D., Fitriana, I., & Sari, P., W. (2015). Acute toxicity testing of herbal remedies in mice based on the Organization for Economic Co-operation and Development (OECD): *Jurnal Sain Veteriner. 33*(2), 234-239.

Siagian, I., J., Purnomo, H., & Ediati, S. (2022). Study In silico compounds in sea cucumbers as immunomodulators: *Journal of Pharmaceutical And Sciences, 5*(1), 33-41.

Sulastra, C,. S., Khaerati, K., & Ihwan. (2020). Acute toxicity and lethal dose (LD50) of purple uwi banggai ethanol extract (*Dioscorea alata* L.) in white rats (*Rattus norvegicus*): *Jurnal Ilmiah Medicamento,* 6(1), 10-14.

Sumaryada, T., Arwansyah., Roslia, A., W., Ambarsari, L., & Kartono, A. (2016). Molecular docking simulation of mangostin derivatives and curcuminoid on maltase-glucoamylase target for searching anti-diabetes drug candidates. Di dalam: 2016 1st International Conference on Biomedical Engineering (IBIOMED), 2016 Okt 5-6, Yogyakarta, Indonesia.

Syabana, M., A., Yuliana, N., D., Batubara, I., & Fardiaz, D. (2021a). α-glukosidase inhibitors from *Syzygium polyanthum* (Wight) Walp leaves as revealed by metabolomics and in silico approaches: *Journal of Ethnopharmacology, 282*,114618.

Syabana, M.,A., Yuliana, N., D., Batubara, I., & Fardiaz, D. (2021b). Characterization of antioxidant compound from *Syzygium polyanthum* leaves extract using UHPLC-HRMS: *Journal of Ethnopharmacology, 16*(1), 38 45.

Tallei, T., E., Tumilaar, S., G., Niode, N., J., Fatimawali, Kepel, B., J., Idroes, R., Effendi, Y., Sakib, S., A., & Emran, T. B. (2020). Potential of plant bioactive compounds as SARS-CoV-2 main protease (Mpro) and spike (S) glycoprotein inhibitors: a molecular docking study: *Scientifica,* (*6307457*), 1-18.

Volkamer, A., Kuhn, D., Rippmann, F., & Rarey, M. (2012). Dogsitescorer: A web server for automatic binding site prediction, analysis and druggability assessment: *Bioinformatics*, *28*(15), 2074-2075.

World, Health, Organization. (2021). Weekly Epidemiological Update on COVID-19 (2021). Diakses dari https://www.who.int/publications/m/item/weekly-epidemiological-update-on-covid-19-$-$10-august-2021. [12 November, 2022]

Wu, Y., C., Chen, C., S., & Chan, Y. J. (2020) The outbreak of COVID-19: an overview: *Journal of the Chinese Medical Association*, *83*(3), 217-220.

Yuan, S., Chan, H., C., S., & Hu, Z. (2017). Using PyMOL as a platform for computational drug design. *Wiley Interdisciplinary. Reviews: Computational Molecular Science, 7*(2), 1-10.

Zhu, C., Gao, Y., Li, H., Meng, S., Li, L., Fransisco, J., S., & Zeng, X. C. (2016). Characterizing hydrophobicity of amino acid side chains in a protein environment via measuring contact angle of a water nanodroplet on planar peptide network: *Proceedings of the National Academy of Sciences, 113*(46), 12946-12951.